Mesoscopic Coarse-Grained Simulations of Lysozyme Adsorption

ARTICLE *in* THE JOURNAL OF PHYSICAL CHEMISTRY B · MAY 2014

Impact Factor: 3.3 · DOI: 10.1021/jp409326f · Source: PubMed

3 AUTHORS, INCLUDING:

Jian Zhou
South China University of Technology
84 PUBLICATIONS **1,593** CITATIONS

JPCBFK

MAY 1, 2014
VOLUME 118
NUMBER 17

pubs.acs.org/JPCB

THE JOURNAL OF PHYSICAL CHEMISTRY B

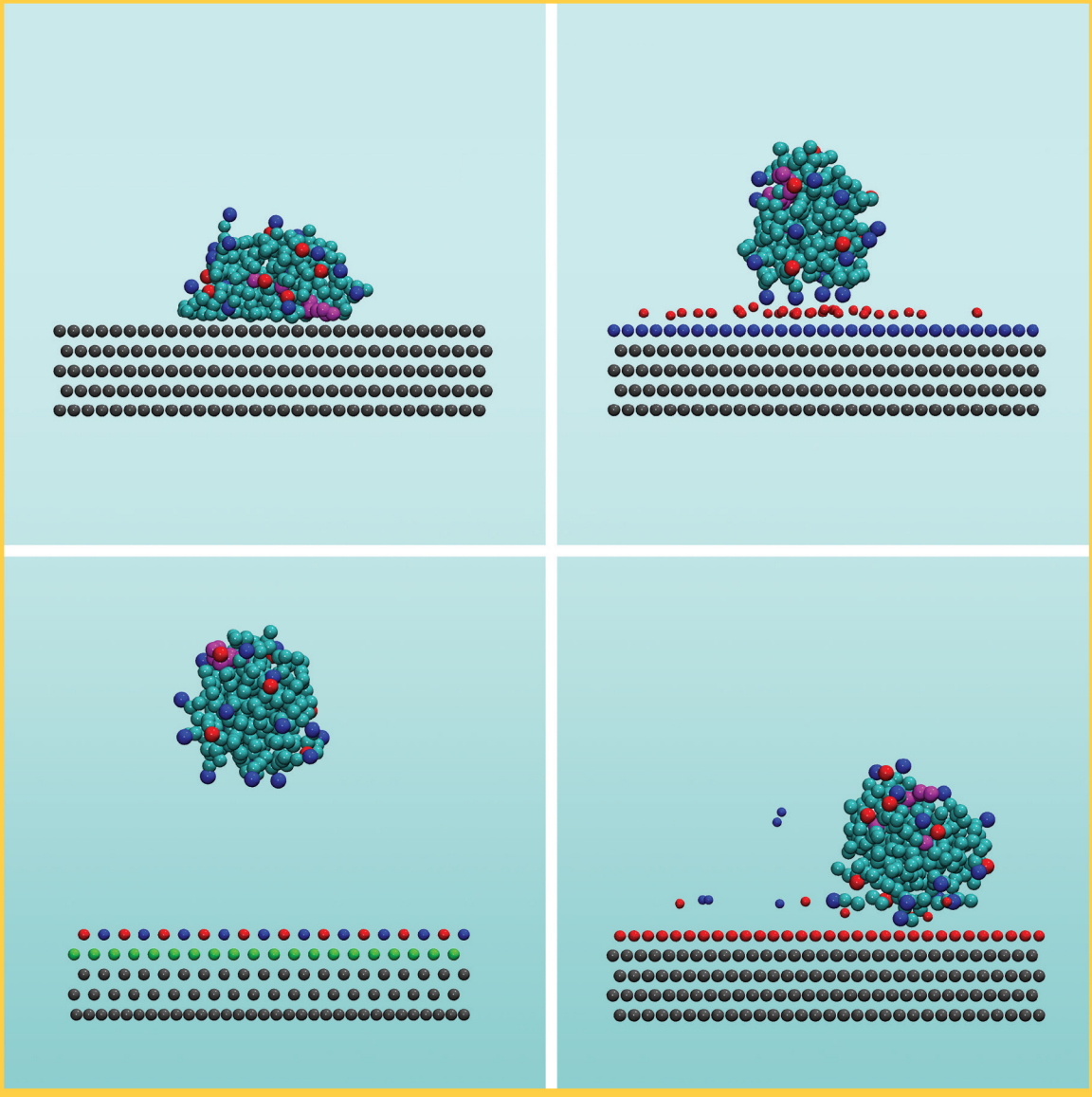

Lysozyme Adsorption on Different Surfaces by Mesoscopic Coarse-Grained Simulations (see page 5A)

BIOPHYSICAL CHEMISTRY, BIOMATERIALS, LIQUIDS, AND SOFT MATTER

ACS Publications
Most Trusted. Most Cited. Most Read.

www.acs.org

THE JOURNAL OF PHYSICAL CHEMISTRY B

Article

pubs.acs.org/JPCB

Mesoscopic Coarse-Grained Simulations of Lysozyme Adsorption

Gaobo Yu, Jie Liu, and Jian Zhou*

School of Chemistry and Chemical Engineering, South China University of Technology, Guangzhou, Guangdong 510640, China

ABSTRACT: Coarse-grained simulations are adopted to study the adsorption behavior of lysozyme on different (hydrophobic, neutral hydrophilic, zwitterionic, negatively charged, and positively charged) surfaces at the mesoscopic microsecond time scale (1.2 μs). Simulation results indicate the following: (i) the conformation change of lysozyme on the hydrophobic surface is bigger than any other studied surfaces; (ii) the active sites of lysozyme are faced to the hydrophobic surface with a "top end-on" orientation, while they are exposed to the liquid phase on the hydrophilic surface with a "back-on" orientation; (iii) the neutral hydrophilic surface can induce the adsorption of lysozyme, while the nonspecific protein adsorption can be resisted by the zwitterionic surface; (iv) when the solution ionic strength is low, lysozyme can anchor on the negatively charged surface easily but cannot adsorb on the positively charged surface; (v) when the solution ionic strength is high, the positively charged lysozyme can also adsorb on the like-charged surface; (vi) the major positive potential center of lysozyme, especially the residue ARG128, plays a vital role in leading the adsorption of lysozyme on charged surfaces; (vii) when the ionic strength is high, a counterion layer is formed above the positively charged surface, which is the key factor why lysozyme can adsorb on a like-charged surface. The coarse-grained method based on the MARTINI force field for proteins and the BMW water model could provide an efficient way to understand protein interfacial adsorption behavior at a greater length scale and time scale.

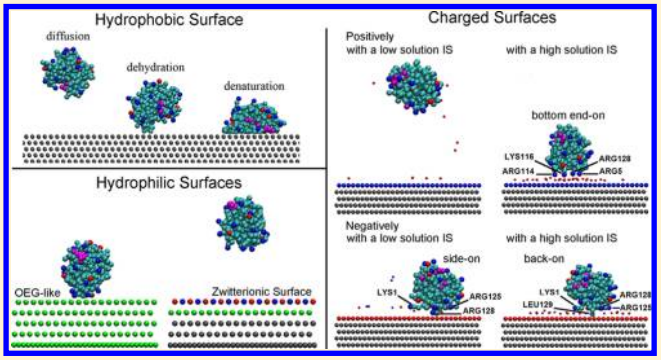

I. INTRODUCTION

Interfacial protein adsorption has stimulated a huge research interest in various areas,[1] such as medicine, pharmaceutical sciences, analytical sciences, biotechnology, cell biology, and biophysics. Among them, there are two major concerns: one is the oriented immobilization,[2−5] and the other is antifouling.[6−8] The mechanism of protein adsorption is still far from being completely understood because various factors and interactions[9−11] affect this complicated process.

A series of experimental techniques[1,12−14] and theoretical models[1,15−18] have been widely used to explore the protein adsorption; however, these explorations cannot directly obtain the molecular details of protein adsorption. An increasingly important access to study protein adsorption events at the molecular scale is the computational approach,[19−22] especially the molecular dynamics (MD) method. It[23] can directly investigate the dynamic process of protein adsorption at the microscopic level.[24] Jiang and co-workers[25−28] performed a combination of MC and MD simulations to study a series of SAMs' resistance to protein adsorption and gave insights into the antifouling mechanism. They showed that, although both the zwitterionic and neutral hydrophilic surfaces are antifouling, the former binds water by ion solvation, while the latter is by hydrogen bonding. Kubiak and Mulheran[29−31] investigated the mechanism of lysozyme adsorption on a negatively charged, hydrophilic surface using atomistic MD simulations. They suggested that the most crucial adsorption site was ARG128 and the driving force of the adsorption was the electrostatics. However, they figured out that electrostatics alone might not be sufficient to drive protein adsorption and immobilization on a charged surface, while the flexibility of protein at the terminal face is also important. Recently, Wei et al.[32] investigated the adsorption of lysozyme on a polyethylene (PE) surface in great detail via full atomistic MD simulations with explicit solvent. They found out that the presence of surfaces could change the hydration only in a sufficiently long simulation time by MD. Thus, they proposed that the long simulation was needed in order to gain a complete understanding of the adsorption process. Subsequently, Wei et al.[33] showed the lysozyme orientation-dependent adsorption behavior, including the initial diffusion and water depletion, and also highlighted the effects of protein and substrate surface hydration on protein adsorption.

Despite the advance in computer power and simulation algorithms, the atomistic simulations are still limited to systems containing tens to hundreds of thousands of atoms or undergoing a sub-microsecond time scale. Many biologically interesting phenomena are beyond the capabilities of atomistic simulations, including the whole process of protein adsorption, protein unfolding, and the formation of higher-order protein complexes. Consequently, we need to simplify the model when simulating these motions. The motivation of this work is to further extend the coarse-grained (CG) method based on the

Received: September 18, 2013
Revised: February 19, 2014
Published: March 5, 2014

MARTINI force field for proteins[34,35] and the BMW water model[36,37] to study protein adsorption on solid surfaces. Thus, the bottleneck of traditional MD simulation in the microscopic nanosecond time scale could be broken; the protein adsorption could be understood at the mesoscopic microsecond time scale.

CG models,[38,39] which allow simulations to be run on larger systems and longer time scales and can preserve basic structural detail of proteins, are an attractive alternative to atomistic models. One of the most popular CG models is the MARTINI force field,[34,35,40−43] which is 3 orders of magnitude more efficient than atomistic models.[35] Instead of focusing on an accurate reproduction of structural details of a particular state for a specific system, Marrink and co-workers developed the MARTINI force field for simulation of biomolecules[34,35,40,44,45] and various other systems.[46−49]

However, MARTINI water beads, just like many other nonelectrostatic water models, do not bear charges, and consequently are blind to electrostatic fields and polarization effects.[42] Because of this, problems arise at the interfaces between water and other phases and in the vicinity of charged particles.[42] Therefore, Wu et al.[36,37] recently developed a modified MARTINI force field, called BMW-MARTINI, which could deal with electrostatic interactions more realistically. By BMW-MARTINI, the dipole potential at the membrane−water interface is in quantitative agreement with experiments and polarizable atomistic simulation results.[37] That is to say, BMW-MARTINI has overcome the significant drawback of these nonelectrostatic water models and could be applied to predict the properties at the interfaces. In addition, BMW-MARTINI is 6 times more expensive than the nonelectrostatic MARTINI water and 2 orders of magnitude more efficient than atomistic models.[37]

In the present work, we applied the aforementioned BMW-MARTINI force field to explore the whole adsorption process and adsorption mechanisms of lysozyme on different (hydrophobic, neutral hydrophilic, zwitterionic, negatively charged, and positively charged) surfaces. Lysozyme, a basic protein of low molecular weight with ellipsoid shape, has long been used as a model protein to study the enzyme kinetics, spatial conformation, and molecular immunology. Besides, abundant experimental, theoretical,[15−17] and computational[4,25−33,50−57] studies of lysozyme adsorption are available for comparison. Therefore, we choose lysozyme as the model protein in this work.

This paper is organized as follows: In section II, we briefly present the method, models, and simulation details. Section III contains a summary of our major results; this section is divided into three parts. In the first part (section IIIA), adsorption processes of lysozyme on hydrophobic/hydrophilic surfaces are presented and discussed. In the second part (section IIIB), we show the different antifouling mechanisms between the zwitterionic surface and the neutral hydrophilic surface. In the third part (section IIIC), we display a variety of molecular details of lysozyme adsorption on negatively charged and positively charged surfaces, with special focus on the influence of ionic strength. Finally, in section IV, the conclusions are offered.

II. COMPUTATION METHODS

Models and Force Fields. All systems were simulated by the BMW-MARTINI force field,[37] which was developed on the basis of the MARTINI (version 2.1) force field[34,35] and BMW water model.[36]

The crystal structure of lysozyme in Figure 1a is taken from the Protein Data Bank (PDB code: 1HEL). The CG structure

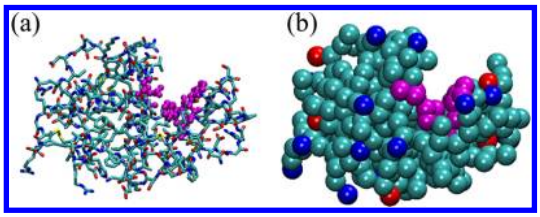

Figure 1. Structural models of lysozyme: (a) atomistic model; (b) CG model. The positively charged atoms/beads are presented in blue, and the negatively charged atoms/beads are presented in red. The magenta part is for the active cleft of lysozyme, and the cyan atoms/beads are for the remainder part. The same coloring scheme of lysozyme is used throughout the manuscript.

of lysozyme is obtained by using the publicly available "martinize.py" script at the MARTINI Web site, as shown in Figure 1b. The backbone structure, main chemical properties of side chains, and secondary structures of protein are preserved after CG mapping in the MARTINI force field.[35,58] In this work, we have tested that, with elastic network constraints, the lysozyme behaves more rigid, which make no difference when it is adsorbed on different surfaces or in bulk. To investigate the relative conformation changes of lysozyme on different surfaces, the elastic network constraints were not used. Moreover, in the BMW-MARTINI force field,[37] the types AC_1 and AC_2 in the original MARTINI[34,35] are replaced by C_1 and C_2; the original MARTINI Q_a is replaced by AQ_a for anions (Cl^-) and peptide C-ter; new subtypes are added for amino acids to introduce additional flexibility: RQ_d for the guanidinium group in arginine and AQ_a for aspartate and glutamate. To mimic the chemical property of different self-assembled monolayer (SAM) surfaces, a simplified processing is taken through a four-to-one mapping (i.e., on average four heavy atoms are represented by a single interaction center).[34] Different simplified SAM-like surfaces studied in this work are listed in Table 1. The built surfaces are SAM-like, while not SAM surfaces; both of them could provide different surface chemistries. To get a comparable baseline of surfaces, all surface beads were fixed during the whole simulation, so they might look ordered. In addition, lysozyme in bulk without surface is also employed as a reference system to be compared with adsorbed protein on different surfaces. Furthermore, on different surfaces, the preferred orientation of the same protein is different. Therefore, to choose the preferred orientation as the initial orientation for the CGMD simulations is an efficient way to study protein adsorption. The lysozyme orientation in Zheng et al.'s MD study[25] was used as the initial orientation of lysozyme on hydrophobic and neutral hydrophilic surfaces, while for negatively charged and positively charged surfaces, the initial orientations were adopted from our previous PTMC study.[4] Besides that, a random initial orientation is adopted for the zwitterionic surface, since this is not a key factor in antifouling study.

The potential energy (U_{tot}) (eq 1) is comprised of the van der Waals (VDW) interaction energy (U_{vdw}) and the electrostatic interaction energy (U_{ele}).

$$U_{tot} = U_{vdw} + U_{ele} \quad (1)$$

In the original MARTINI force field,[34,35] the VDW interaction energy is calculated by the Lennard-Jones potential (eq 2) model:

dx.doi.org/10.1021/jp409326f | J. Phys. Chem. B 2014, 118, 4451−4460

Table 1. CG Surfaces in Present Study

surfaces	molecule in self-assembled monolayer	CG mapping
hydrophobic (CH_3-SAM-like)	$-(CH_2)_{19}CH_3$	$C_1-C_1-C_1-C_1-C_1$
neutral hydrophilic (OH-SAM-like)	$-(CH_2)_{19}OH$	$C_1-C_1-C_1-C_1-P_1$
neutral hydrophilic (OEG-like)	$-(OCH_2CH_2)_5OH$	$P_4-P_4-P_4-P_4-P_4$
zwitterionic (sulfonic betaine-like (SB-like))	$-(CH_2)_{11}N^+(CH_3)_2CH_2SO_3^-$	$C_1-C_1-C_1-P_5-Q_a$
		$C_1-C_1-C_1-P_5-Q_d$
negatively charged (N)	$-(CH_2)_{17}COOH$	$C_1-C_1-C_1-C_1-Q_a$
positively charged (P)	$-(CH_2)_{19}NH_2$	$C_1-C_1-C_1-C_1-Q_d$

Table 2. Averaged Properties of Studied Systems by CGMD Simulations

system	IS (M)	RMSD[a] (nm)	COM-dis (nm)	MIN-dis (nm)	cos θ	orientation[4]
bulk	0.015	0.45 ± 0.01				
CH_3-SAM-like	0.015	0.67 ± 0.02	1.29 ± 0.02	0.45 ± 0.01	0.73 ± 0.13	top end-on
OH-SAM-like	0.015	0.51 ± 0.01	1.53 ± 0.03	0.46 ± 0.01	0.24 ± 0.09	lower back-on
OEG-like	0.015	0.45 ± 0.02	2.27 ± 0.03	0.49 ± 0.02	−0.60 ± 0.14	left side-on
SB-like	0.015	0.46 ± 0.02	5.76 ± 0.09	4.11 ± 0.18		
P	0.03	0.46 ± 0.01	6.46 ± 0.07	4.64 ± 0.18		
N	0.03	0.44 ± 0.02	2.19 ± 0.02	0.49 ± 0.02	−0.61 ± 0.13	side-on
P-IS	0.8	0.47 ± 0.01	2.64 ± 0.04	0.78 ± 0.03	−0.93 ± 0.05	bottom end-on
N-IS	0.8	0.46 ± 0.01	2.38 ± 0.03	0.53 ± 0.05	−0.30 ± 0.15	back-on

[a]The RMSD values displayed in Table 2 are the backbone structural changes between the simulated CG structure of lysozyme and the CG crystal structure of lysozyme. It is defined as RMSD = $(\langle\sum_{i=1}^{N} m_i(r_i - r_{i,\mathrm{ref}})^2\rangle/M)^{1/2}$, where $M = \sum_{i=1}^{N} m_i$, N is the number of the beads, m_i is the mass of bead i, and r_i and $r_{i,\mathrm{ref}}$ are the position of bead i at time t and the reference position, respectively. As Periole and Marrink mentioned, in the MARTINI force field, it may result in an unusually high RMSD of the model with respect to the experimental structure but does not mean it is unfolding.[58] Therefore, even though the MARTINI model would result in a relatively high RMSD of lysozyme, by CGMD with MARTINI, the RMSD values of lysozyme on different surfaces are different. As a result, our CGMD simulations can qualitatively indicate the relative conformational changes of the adsorbed lysozyme on different surfaces.

$$U_{\mathrm{vdw}} = 4\varepsilon_{ij}\left[\left(\frac{\sigma_{ij}}{r}\right)^{12} - \left(\frac{\sigma_{ij}}{r}\right)^{6}\right] \quad (2)$$

while in the BMW-MARTINI force field,[36,37] a modified form of the Born−Mayer−Huggins (BMH)[59,60] potential (eq 3) is used to describe the VDW interaction.

$$U_{\mathrm{vdw}} = \frac{\varepsilon}{1 - \frac{f}{a} - \frac{6-f}{12}}\left\{\frac{6-f}{12}\left(\frac{r_{\mathrm{m}}}{r}\right)^{12} - \left(\frac{r_{\mathrm{m}}}{r}\right)^{6} + \frac{f}{a}\exp\left[a\left(1 - \frac{r}{r_{\mathrm{m}}}\right)\right]\right\} \quad (3)$$

In addition to the VDW interaction, charged groups interact via a shifted Coulombic potential energy function (eq 4) in the original MARTINI force field, while electrostatic interactions in the BMW-MARTINI model are calculated using the particle mesh Ewald (PME)[61,62] method.

$$U_{\mathrm{ele}} = \frac{q_i q_j}{4\pi\varepsilon_0\varepsilon_1 r} \quad (4)$$

It should be stressed herein that the original MARTINI force field[34,35] utilizes a relative dielectric constant (ε_1) of 15 for screening electrostatic interactions and consequently the original MARTINI force field may be less accurate to describe interactions between charged species. However, in the BMW-MARTINI model,[36,37] the ε_1 is adjusted to 1.3.

Simulation Details. The simulation protocols used for this work are largely the same as for BMW-MARTINI works.[36,37] CGMD simulations in the NVT ensemble were performed to examine the adsorption behaviors of lysozyme, using the GROMACS 4.5.5 package.[63] It is worth noting that, because of the smoothed energy barrier in the MARTINI force field, the effective time that the system has gone through is 4 times longer than the simulation sampling time. A 20 fs time step is used to integrate the equations of motion with the half leapfrog algorithm. A 1.2 μs CGMD simulation was performed for each system. The simulation box size is 7.52 × 7.52 × 10 nm^3, and the water density in this work is about 1.041 g/cm^3, which well agrees with that, 1.047 g/cm^3, by Wu et al.[36] The neighbor list is updated every 10 steps with a cutoff of 1.4 nm. PME with a spacing of 0.2 nm and ε_r = 1.3 are applied for electrostatics. For all LJ interactions, r_{shift} = 0.9 nm and r_{cut} = 1.2 nm, while the switch scheme (r_{shift} = 0.9 nm and r_{cut} = 1.4 nm) is used for water−water VDW interactions. The initial velocities of beads are generated on the basis of the Maxwell distribution at system temperature, which is controlled at 300 K by the Berendsen method[64] with a time constant of 0.2 ps. For structure and electrostatic potential visualization, the visual molecular dynamics (VMD)[65] and chimera[66] programs are used, respectively.

III. RESULTS AND DISCUSSION

The adsorption behaviors of lysozyme on six surfaces (i.e., hydrophobic (CH_3-SAM-like), neutral hydrophilic (OH-SAM-like), neutral hydrophilic (OEG-like-SAM), zwitterionic (SB-like-SAM), negatively charged, and positively charged surfaces) are investigated by CGMD simulations with the BMW-MARTINI force field. For comparison, proteins in the bulk solution are also studied. Additionally, the influence of ionic strength (IS) is taken into account for charged surfaces. The optimal orientation, root-mean-square deviation (RMSD), mass center distance, and minimal distance between protein and surfaces are calculated during the CGMD simulations.

dx.doi.org/10.1021/jp409326f | J. Phys. Chem. B 2014, 118, 4451−4460

Simulation results are summarized in Table 2 and Figures 2−12.

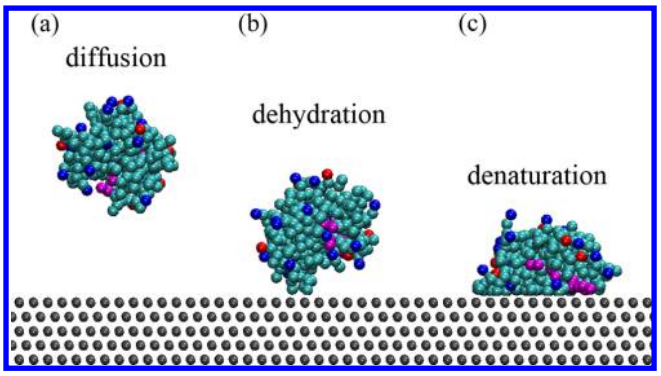

Figure 2. A three-step process for lysozyme adsorption on a hydrophobic (CH_3-SAM-like) surface: (a) the state before diffusion; (b) the state during dehydration; (c) the state after denaturation. The surface in gray is for the hydrophobic (CH_3-SAM-like) surface (i.e., the bead in gray is hydrophobic).

A. Lysozyme Adsorption on Hydrophobic and Hydrophilic Surfaces. In this section, CH_3-SAM-like and OH-SAM-like surfaces were reduced as hydrophobic and neutral hydrophilic surfaces, respectively.

For the hydrophobic surface, as shown in Figure 2, a three-step process (i.e., diffusion, dehydration, and denaturation) of lysozyme adsorption is found by CGMD simulations, which was similarly found by Wei et al.[32] through atomistic MD simulations. First, with a preferred initial orientation, the lysozyme starts to approach the hydrophobic surface from the solution (i.e., diffusion stage), which is a rapid stage. Moreover, it can be treated as the reorientation stage ended with the touchdown. Then, it comes to the dehydration stage. During this stage, the water molecules trapped between the lysozyme and the hydrophobic surface need to be removed before the protein comes into full contact with the surface.[32] During these two stages, the backbone structure of protein does not significantly change and the cleft of lysozyme as shown in Figure 1b could still be observed in Figure 2a and b. Finally, it comes to the denaturation stage, which illustrates the conformational changes of protein during the adsorption. The unfolding, stretching, and migration processes occurred during this stage. Due to the hydrophobic interaction between the protein and the nonpolar surface, the hydrophobic residues, which are located inside the lysozyme in the native, are exposed to the surface. Thus, the active cleft (i.e., GLU35, ASP52, TRP62, TRP63, and ASP101, which are presented in magenta in Figure 2) within the lysozyme contacts with the hydrophobic surface directly.

By comparing Figures 3 and 4, we find that, during 200−500 ns, the mass center distance between the protein and the surface as well as the RMSD of lysozyme have a consistent change. The mass center distance declines slowly from 1.52 to 1.31 nm (Figure 3); meanwhile, the RMSD has a corresponding increase from 0.47 to 0.68 nm (Figure 4). These results suggest that a dramatic conformation change has happened during 200−500 ns. After that, lysozyme has reached the steady adsorption state, as shown in Figure 2c. This adsorption state, which is beyond the microsecond time scale, is difficult to be observed in all-atom molecule dynamics

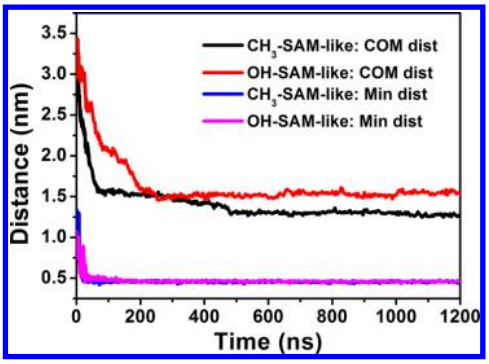

Figure 3. Mass center distance and min-distance of lysozyme on the hydrophobic (CH_3-SAM-like) surface and the hydrophilic (OH-SAM-like) surface. The mass center distances of lysozyme on the hydrophobic and hydrophilic surfaces are presented in black and red, respectively. The min-distances of lysozyme on the hydrophobic and hydrophilic surfaces are presented in blue and magenta, respectively.

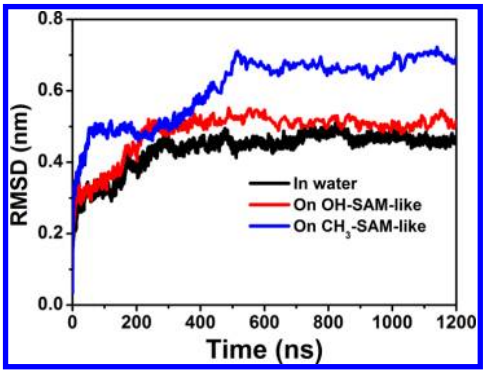

Figure 4. RMSD evolution of the lysozyme backbone on hydrophobic (CH_3-SAM-like) and hydrophilic (OH-SAM-like) surfaces as a function of time. The RMSD evolution of lysozyme in water is presented with the black line. The RMSD evolutions of lysozyme on the hydrophobic (CH_3-SAM-like) surface and on the hydrophilic (OH-SAM-like) surface are presented with blue and red lines, respectively.

(AAMD). Thus, it is necessary to perform CGMD to investigate the whole process of protein adsorption.

The coarse-grained protein is not as stable with the atomistic model in water, but it becomes further unstable in the presence of a CH_3-SAM-like surface. From Table 2 and Figure 4, it could be seen that the RMSD of lysozyme adsorbed on the hydrophilic surface was smaller than that on the hydrophobic surface, which was based on the analysis of the latter 600 ns trajectory. The results indicated that the structural changes on the hydrophilic surface are less than that on the hydrophobic surface. The internal reason is that the hydrophobic residues are located inside the protein, while the hydrophilic ones are outside. Therefore, the exposure of hydrophobic residues can only occur on the hydrophobic surface. Thus, the lysozyme on the hydrophobic surface is easily denatured while the activity of protein on the hydrophilic surface could be preserved. As the RMSD just reveals the overall conformation change of adsorbed proteins, the local structure deviation or the change of secondary structure cannot be observed. Thus, we further analyze the root-mean-square fluctuation (RMSF) to illustrate the local conformation changes. As is shown in Figure 5, it also could be found that the RMSF of lysozyme adsorbed on the hydrophilic surface is smaller than that on the hydrophobic

dx.doi.org/10.1021/jp409326f | J. Phys. Chem. B 2014, 118, 4451−4460

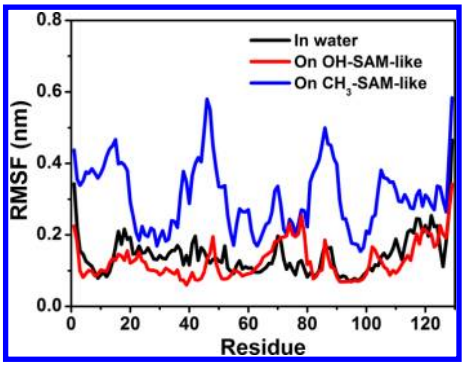

Figure 5. The RMSF of lysozyme adsorbed on hydrophobic (CH_3-SAM-like) and hydrophilic (OH-SAM-like) surfaces. The RMSF evolution of lysozyme in water is presented with the black line. The RMSF evolutions of lysozyme on the hydrophobic (CH_3-SAM-like) surface and on the hydrophilic (OH-SAM-like) surface are presented with blue and red lines, respectively.

surface. The RMSFs of the terminal residues always have a relatively larger value. Moreover, on the hydrophobic surface, most fluctuations of the RMSF are contributed by the terminal residues and these exposure residues (LEU17, ALA42, ASN46, LEU84, ILE88, and MET105), which are hydrophobic residues located in turn or without secondary structure.

The final adsorbed states of lysozyme on hydrophobic and hydrophilic surfaces are displayed in Figure 6. The figure

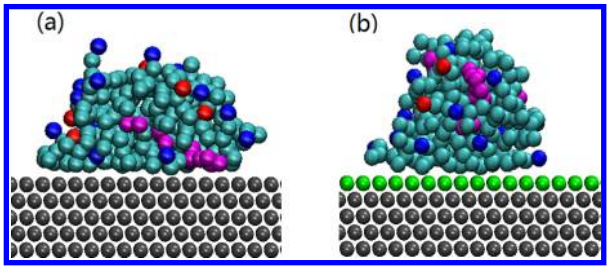

Figure 6. The final adsorption states of lysozyme on neutral surfaces: (a) CH_3-SAM-like, hydrophobic; (b) OH-SAM-like, hydrophilic. The surface with five gray layers is for the hydrophobic (CH_3-SAM-like) surface, while the surface with a top layer in green and four bottom layers in gray is for the hydrophilic (OH-SAM-like) surface (i.e., the bead in green is hydrophilic).

showed that the orientation of lysozyme on the hydrophobic surface is "top end-on" (as shown in Figure 6a). Moreover, lysozyme is adsorbed to the hydrophobic surface in an orientation with its active cleft down against the surface. As we have mentioned above, the conformation of lysozyme on the hydrophobic surface undergoes a dramatic change. These all indicate that lysozyme loses its bioactivity when it is adsorbed on a hydrophobic surface. However, the activity can be maintained much better on a hydrophilic surface due to the "back-on" orientation of the lysozyme (as shown in Figure 6b), which exposes the active cleft to the solution. Fears et al.[67] also found that, when lysozyme was adsorbed on a hydrophobic CH_3-SAM-like surface, the bioactive site of lysozyme could not be detected; however, it could be detected when the lysozyme was adsorbed on a hydrophilic OH-SAM-like surface.

B. The Neutral Hydrophilic and Zwitterionic Surfaces for Antifouling. In this section, an oligo-(ethylene glycol)-like (OEG-like) surface and a sulfonic betaine-like (SB-like) surface has been employed as a neutral strongly hydrophilic and a zwitterionic surface, respectively. Previous studies[25−27,68] of these two materials suggested that they both had a good resistance performance for proteins. For the OEG-like surface, the nonspecific protein adsorption could be induced after a long time, while the SB-like surface was still antifouling.[69] Therefore, we mimic these two materials by CGMD simulations based on the BMW-MARTINI force field to explore their different antifouling mechanisms. The CGMD results of this part are shown in Table 2 and Figures 7 and 8.

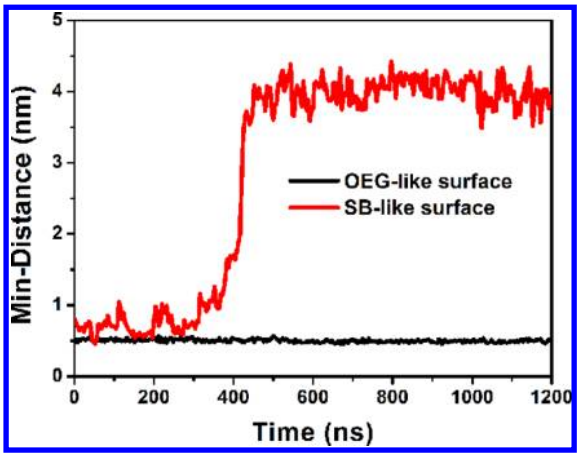

Figure 7. Closest distance between lysozyme and antifouling surfaces as a function of time. The min-distances of lysozyme on the strongly hydrophilic (OEG-like) surface and the zwitterionic (SB-like) surface are presented with black and red lines, respectively.

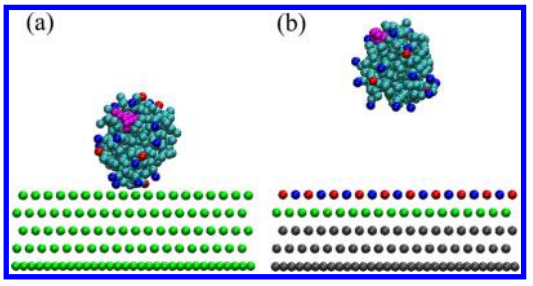

Figure 8. Final adsorption states of lysozyme on antifouling surfaces: (a) OEG-like surface, strongly hydrophilic; (b) SB-like surface, zwitterionic. The surface with a top layer alternating with red and blue beads, one green layer and three gray layers is for the zwitterionic (SB-like) surface, while the surface with five layers in green is for the strong hydrophilic (OEG-like) surface. Additionally, the bead in red is negatively charged, and that in blue is positively charged.

From Figures 7 and 8, we can see a clear distinction for the lysozyme adsorption states between OEG-like and SB-like surfaces. As we have mentioned above, the protein can adsorb on a short chain OEG-like-SAM after a long-term process.[69] For a zwitterionic surface, the protein keeps away from the surface during the whole simulation. The hydration layer above the SB-like-SAM is bound by ion solvation, which is particularly stronger than that by hydrogen bond.[68−70] Thus, the lysozyme cannot adsorb on SB-like-SAM, which is presented in our simulation. It is also indicated that the BMW-MARTINI force field is suitable for the illustration of both antifouling materials.

The difference between OEG-like and OH-SAM-like surfaces is presented in Table 2 by RMSD and mass center distance. Since the hydrophilic property of OEG-like surface is stronger than that of OH-SAM-like surface, the hydration layer on OEG-

dx.doi.org/10.1021/jp409326f | J. Phys. Chem. B 2014, 118, 4451−4460

like surface is more stable than that on OH-SAM-like surface. Thus, it is hard for protein to move the water away from the OEG-like surface. In other words, the lysozyme cannot adsorb on the OEG-like surface stably. The RMSD in Table 2 has revealed that the lysozyme on the OEG-like surface has the same value as in the bulk, while that on the OH-SAM-like surface presents a slight difference. It means that the protein keeps its native form when it is adsorbed on the OEG-like surface. Meanwhile, the center mass distance between the lysozyme and OEG-like surface is also larger than that between lysozyme and the OH-SAM-like surface. This also indicates that lysozyme adsorbs unstably on the OEG-like surface.

C. Lysozyme Adsorption on Negatively Charged and Positively Charged Surfaces. In this section, we investigate the lysozyme adsorption on oppositely charged surfaces. Particularly, we also investigate the influence of solution IS. Therefore, there are a total of four systems in this part: a positively charged surface with a low solution IS (0.03 mol/L) (P), a negatively charged surface with a low solution IS (0.03 mol/L) (N), a positively charged surface with a high solution IS (0.8 mol/L) (P-IS), and a negatively charged surface with a high solution IS (0.8 mol/L) (N-IS).

The Relationship between Solution Ionic Strength and Surface Distribution of Ions. As is shown in Figure 9 (P, N, P-IS, N-IS), there are only 16 ions that exist in the systems of P and N. Therefore, it is hard to form a stable counterion layer above the charged surface. However, in both systems of P-IS and N-IS, an ion layer near the surface appears (Figure 9), due to the electrostatic attraction. Interestingly, the ion layer in P-IS is composed almost by Cl^- (Figure 9b); however, it is formed by the mixture of Na^+ and Cl^- in system N-IS (Figure 9d). The profile in Figure 10 also shows that there is a Cl^- layer formed above the positively charged surface, whereas there is a mixed Na^+ and Cl^- layer above the negatively charged surface. The possible reason is that the ion hydration of Na^+ is stronger than that of Cl^-,[71] i.e., Na^+ tends to stay in the bulk while Cl^- is more inclined near the interface.[72−74] Interestingly, our analysis below would point out that the electric double layer is a key factor to understand the adsorption mechanism of the protein on different systems.

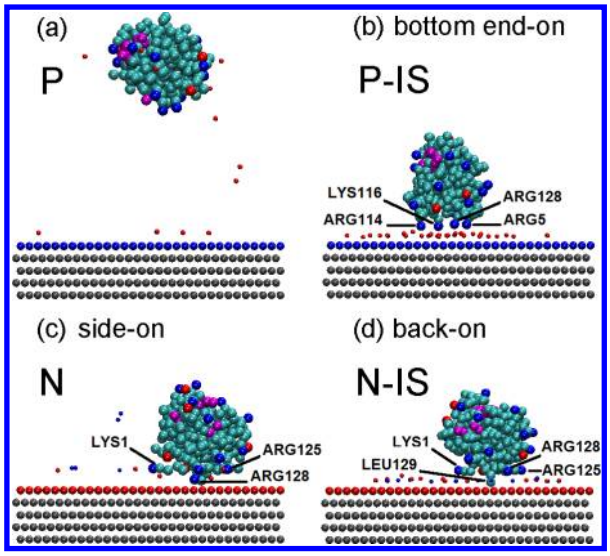

Figure 9. Final adsorption states of lysozyme on charged surfaces: (a) positively charged surface with a low solution IS (0.03 mol/L) (P); (b) positively charged surface with a high solution IS (0.8 mol/L) (P-IS); (c) negatively charged surface with a low solution IS (0.03 mol/L) (N); (d) negatively charged surface with a high solution IS (0.8 mol/L) (N-IS). The surface with a top layer in blue and four bottom layers in gray is for the positively charged surface, while that with a top layer in red and four gray layers is for the negatively charged surface. In addition, the smaller beads in red are for Cl^-, while those in blue are for Na^+.

To a certain extent, the mechanism of protein adsorption on charged surfaces can be explained by the DLVO theory.[75,76] For low ionic strength systems (P and N), there is no effective electric double layer around the protein and the surface. Thus, the attraction and repulsion between proteins and surfaces directly depend on the electrostatic and van der Waals interactions. In system P, the lysozyme and the positively charged surface are both positive and the electrostatic repulsion beats the van der Waals attraction; therefore, there is no lysozyme adsorption. On the contrary, for system N, the lysozyme and the negatively charged surface have different electrical properties; hence, the strong electrostatic attraction and the van der Waals attraction between them can drive the lysozyme to adsorb onto the negatively charged surface easily. For high ionic strength systems (P-IS and N-IS), an effective electric double layer can be formed between the protein and the surface. As a result, the electric double layer weakens the electrostatic interactions between lysozyme and surfaces. Therefore, under this circumstance, the competition between the electrostatic interactions caused by the electric double layer and van der Waals attraction determines the adsorption/desorption behavior of proteins on surfaces. For the P-IS system, the interactions between the protein and the counterion layer on the positively charged surface are electrostatic attraction. Therefore, compared with system P, the lysozyme can be adsorbed in system P-IS. For the N-IS system, there is a mixed cation and anion layer above the negatively charged surface, so the adsorption in system N-IS is weaker than that in system N.

Min-Distance between Protein and Surface. According to the min-distance between lysozyme and surfaces (Figure 11), it can be seen that lysozyme can adsorb onto the surface of system N but does not adsorb onto the surface of system P, with the min-distance of 0.8 nm. In systems of P and N, the adsorption is driven by electrostatic interactions between lysozyme and surfaces, since lysozyme is positively charged (+8 e). Thus, in a low IS, lysozyme can only adsorb on the negatively charged surface (N) with a min-distance of 0.47 nm, while it is repelled from the surface in system P owing to the electrostatic repulsion. At a higher IS, lysozyme can adsorb on oppositely charged surfaces both in systems of N-IS and P-IS. It is worth noting that the high IS makes the adsorption process in system N-IS much slower and weaker than that in system N, as shown in Figure 11. Our previous works[3,4] had indicated that, when IS is low, electrostatic interactions dominate the protein adsorption, whereas, at high IS, VDW interactions would gradually become the domination force. From Figure 11 and Table 2, it can be seen that the min-distance between the protein and the surface in system P-IS is about 0.78 nm, which is larger than that in system N-IS (0.53 nm) or system N (0.49 nm). We point out that the primary reason for this phenomenon is the formation of the ion layer, which has been mentioned above. Therefore, in system P-IS, the protein is not directly adsorbed onto the surface but stably adsorbed on the ion layer above the surface. In system N-IS, there is not a perfect ion layer formed above the negatively charged surface,

dx.doi.org/10.1021/jp409326f | J. Phys. Chem. B 2014, 118, 4451−4460

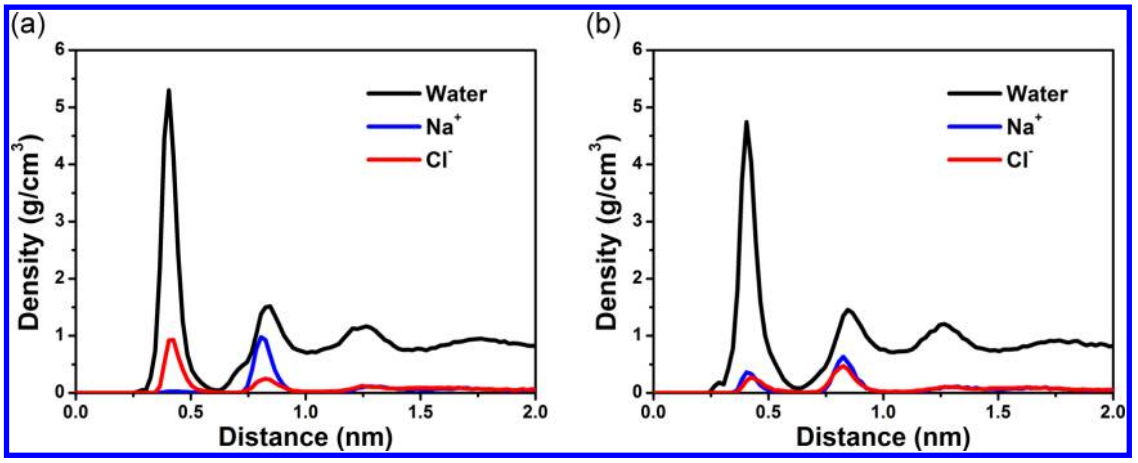

Figure 10. The density distribution profiles of ions (Na^+/Cl^-) and water above the charged surfaces: (a) P-IS; (b) N-IS. The density distribution of the water is presented with a black line. The distributions of the Na^+ and Cl^- are presented in blue and red, respectively.

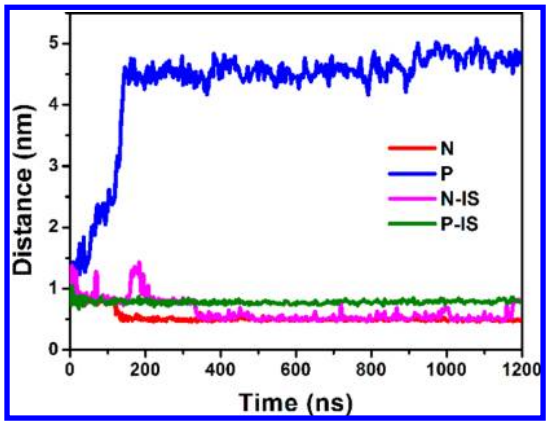

Figure 11. Min-distance between lysozyme and charged surfaces as a function of time. The min-distances between lysozyme and surfaces in N, P, N-IS, and P-IS are presented with red, blue, magenta, and green lines.

so protein can easily penetrate the ion layer and adsorb onto the surface with the same min-distance as that in system N, but the adsorption process is obviously slower than that in system N, since the high IS reduces the strong electrostatic interactions between the protein and the surface.

Binding Sites. As simulation snapshots (Figure 9) show, in systems N and N-IS, the main binding sites are ARG128, whereas, in system P-IS, the main binding sites are ARG128, ARG5, ARG114, and LYS116.

From the plot of min-distance between the key residues and the surface in system N (Figure 12c), the ARG128 first approaches to the water layer (about 0.2 ns) and then it breaks through the water layer to adsorb on the surface directly as an anchoring point (at around 120 ns). Meanwhile, the ARG128 can drive its neighbor LEU129 to penetrate the water layer as another anchoring point (at around 160 ns). Subsequently, LYS1, ARG5, and ARG125 act as the minor residues for protein adsorption, although they do not penetrate the water layer through the whole simulation.

For system N-IS (Figure 12d), ARG128 can also move close to the ion layer at around 20 ns. However, as is discussed above, the strong IS can weaken the electrostatic interactions between the protein and the surface. In other words, the interactions between ARG128 and the negatively charged surface are declined as a result of the strong IS. Therefore, ARG128 does not penetrate the ion layer and the adsorption is unstable. ARG128 is the first residue to move toward the surface; meanwhile, it can induce the adsorption of its neighbor LEU129. No matter if in system N, N-IS, or P-IS (Figure 12), ARG128 is always the key residue for lysozyme adsorption. Just because LEU129 is the neighbor of ARG128, LEU129 also appears in the vicinity of surfaces.

As for system P-IS (Figure 12b), the first residue that adsorbs on the ion layer is ARG128 (within 0.4 ns). Almost at the same time, ARG125 adsorbs onto the surface. After the chloride ion layer forms, some positively charged residues (e.g., ARG5, LYS1, ARG114, and LYS116) around the two established anchoring points (i.e., ARG128 and ARG125) are drawn close to the chloride ion layer. Owing to the chloride ion layer, the repulsive electrostatic interaction between protein and the positively charged surface is screened. Thus, the protein can adsorb on the counterion layer. Finally, we found that there are about five key residues (ARG128, ARG125, ARG5, ARG114, LYS116) acting as the binding site during the protein adsorption. All these key residues do not penetrate the chloride ion layer in system P-IS (Figures 9b and 10a). However, during the whole simulation, lysozyme is adsorbed with more than three anchoring points on the chloride ion layer. Because of the chloride ion layer above the surface, the strong electrostatic repulsion from the surface has been screened; meanwhile, it provides a plane for many other charged residues to anchor. Therefore, the formation of a chloride ion layer is the key factor which induces the lysozyme to have a relatively stronger binding in system P-IS, rather than in system N or N-IS. Moreover, it is worth noting that whether in system N, N-IS, or P-IS, ARG128 always plays a vital role in leading the adsorption of lysozyme. Kubiak and Mulheran[30] figured out the critical role of ARG128 in lysozyme adsorption on a negatively charged solid surface. They suggested that full immobilization only occurred through the strong interaction of ARG128 with the surface, facilitated by the protein's flexibility at the terminal face. Recently, Hung et al.[77] also suggested that amphiphilic amino acids, especially ARG, played a key role in the adsorption of proteins on both hydrophobic and hydrophilic surfaces.

As discussed above, due to the chloride ion layer in system P-IS, we can suggest that, no matter what the system is, N, N-IS, or P-IS, lysozyme always likes to adsorb on the effectively negative potential surface. In addition, the preferred orientation is dominated by a series of positive charged residues (ARG128,

dx.doi.org/10.1021/jp409326f | J. Phys. Chem. B 2014, 118, 4451−4460

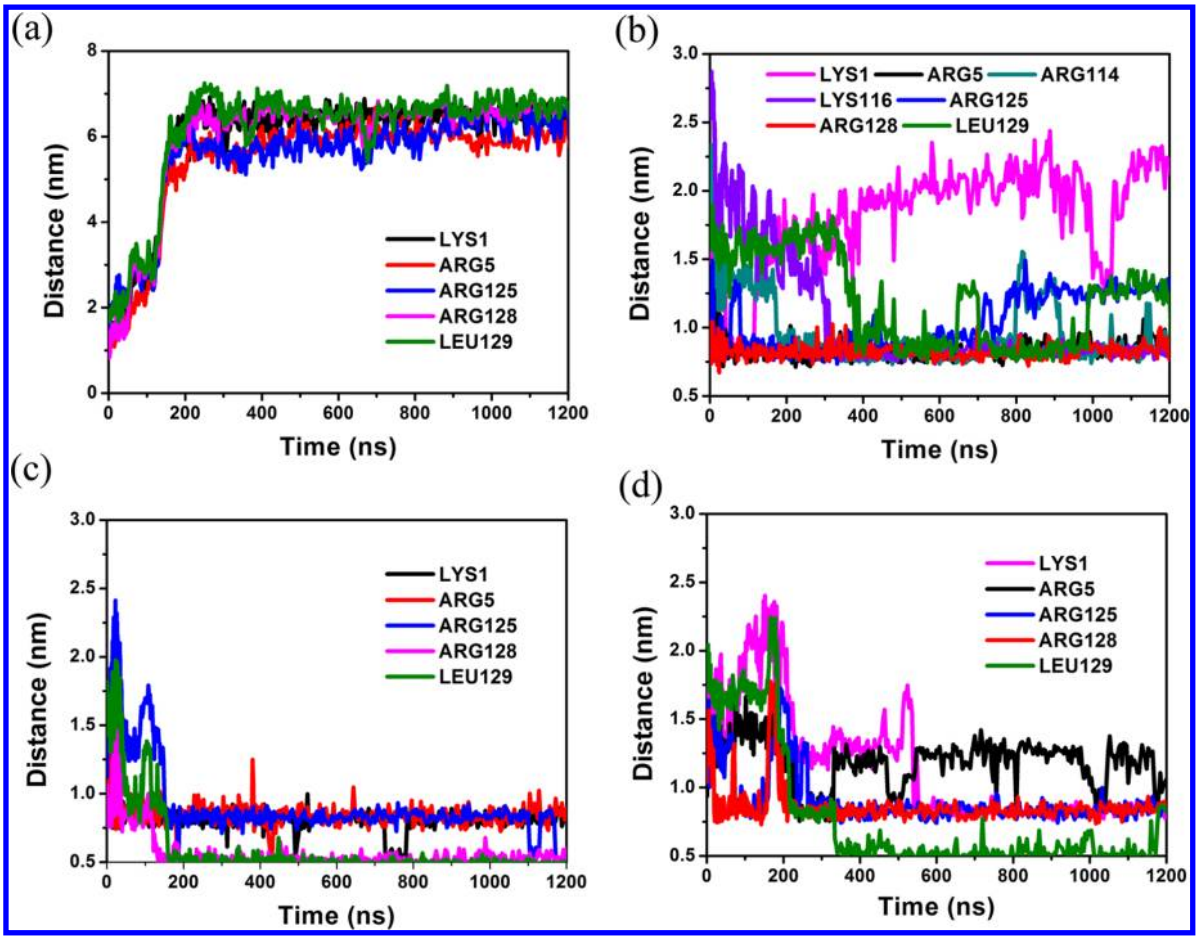

Figure 12. Distance of the key residues' mass center to the surface as a function of time: (a) P; (b) P-IS; (c) N; (d) N-IS. The evolutions of the mass center distance between the surface and binding sites (LYS1, ARG5, ARG125, ARG128, and LEU129) are orderly presented in colored lines (black, red, blue, magenta, and green).

ARG125, ARG5, LYS1), as shown in Figures 9 and 12. Furthermore, it should be pointed out that these positive charged residues are all contained in the major positive potential region (black frame in Figure 13). So many positive residues of lysozyme are gathered in this region, which makes it the dominating center for lysozyme adsorption on the negatively charged surfaces. According to the structure of this patch (Figure 13), we can find that the residue ARG128 is the outward extension of this region. Therefore, while the domination center facilitates the lysozyme penetration into the double layer and adsorption on the surfaces, the residue ARG128 may contribute mostly which is consistent with the discussion above.

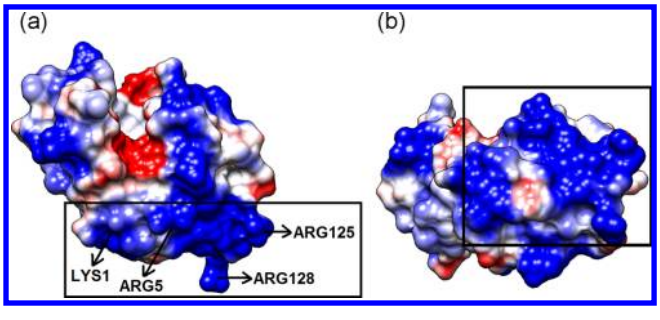

Figure 13. Electrostatic maps of lysozyme: (a) the simulated orientation of lysozyme on a negatively charged surface; (b) bottom view of part a. The region in blue is for part of the positive potential, while that in red is for part of the negative potential. The white region is in neutral potential.

Orientation Distribution. As in our previous work,[4] the orientation angle (θ) and cos θ were calculated for each possible orientation to quantitatively characterize the orientation of adsorbed proteins on the surfaces. The orientation angle is defined as the angle between the unit vector normal to the surface and the unit vector along the dipole of a protein.

Figure 14 has shown the orientation distribution of adsorbed lysozyme in systems N, N-IS, and P-IS. In system N, lysozyme is adsorbed with the preferred "side-on" orientation (cos θ = −0.60), as shown in Figure 9. In system N-IS, the "side-on" orientation turns to be the "back-on" orientation (cos θ = −0.30). This CGMD result is consistent with the experimental results by Dismer et al.[12,13] of lysozyme adsorption on strongly negatively charged resin. Meanwhile, in Figure 14, as IS increases, the orientation distribution in N-IS becomes slightly wider and lower than that in system N. When protein adsorption is driven by electrostatic interactions, it would be favorable for positioning adsorbed protein layer in a uniform orientation, which confirms the electrostatically driven mechanism in controlling protein orientation proposed in our previous simulation works.[3−5] Interestingly, the orientation distribution of protein in system P-IS is much narrower than that in N or N-IS, and the dominant orientation of lysozyme is the "bottom end-on" with cos θ = −0.93, as shown in Figure 14

dx.doi.org/10.1021/jp409326f | J. Phys. Chem. B 2014, 118, 4451−4460

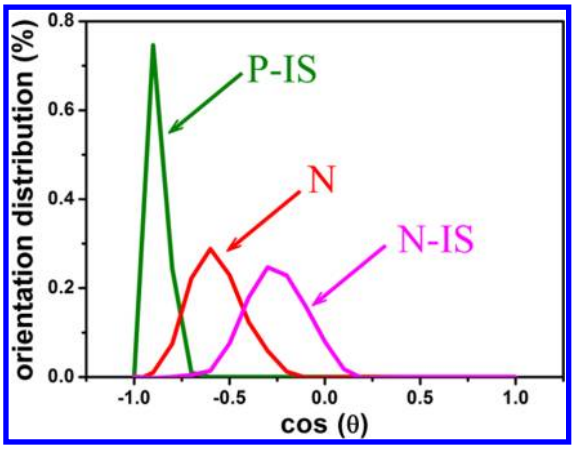

Figure 14. Orientation distributions of lysozyme adsorbed on charged surfaces. The distribution of lysozyme in system N is presented with a red line. The distributions of lysozyme in systems N-IS and P-IS are presented in magenta and green lines, respectively.

and the row of cos θ in Table 2. The narrowest orientation distribution indicates that the adsorption strength in P-IS is the strongest one among the three systems. A possible reason for this phenomenon is that there is usually a water layer above the charged surface.[31,78] That is to say, in most instances (such as systems N and N-IS), lysozyme has to penetrate the water layer in order to adsorb onto the charged surface. However, only few residues can penetrate water and adsorb on the surface directly. Meanwhile, these binding sites are disturbed by the surrounding molecules (water molecules and ions), resulting in the swing of the lysozyme. Thus, the orientation of lysozyme is distributed wider. As the ionic strength increases, the adsorption strength of these binding sites becomes weaker and the orientation distributes relatively wider (i.e., the orientation distribution in system N-IS is relatively wider than that in system N). For system P-IS, lysozyme is adsorbed onto the chloride ion layer which is formed above the positively charged surface. ARG128, ARG5, ARG114, and LYS116 form a relatively flat contacting plane, which makes lysozyme have less probability to swing on the surface. Therefore, the orientation distribution of P-IS is narrower than those of systems N and N-IS.

IV. CONCLUSIONS

CGMD simulations based on the MARTINI protein force field and the BMW water model are first adopted to study the adsorption behavior of lysozyme on different (hydrophobic, neutral hydrophilic, zwitterionic, negatively charged, and positively charged) surfaces at the mesoscopic microsecond time scale for the first time, to the best of our knowledge.

Simulation results indicate the following: (i) the denaturation degree of lysozyme on a hydrophobic surface is greater than that on a hydrophilic surface; (ii) the active sites of lysozyme face the hydrophobic surface with a "top end-on" orientation, while they are exposed to the liquid phase on the hydrophilic surface with a "back-on" orientation; (iii) the neutral hydrophilic surface can induce the adsorption of lysozyme, while the nonspecific protein adsorption can be resisted by the zwitterionic surface; (iv) when the solution ionic strength is low, lysozyme can anchor on the negatively charged surface easily but cannot adsorb on the positively charged surface; (v) as a result of the strong solution ionic strength, the positively charged lysozyme can also adsorb on the like-charged surface (via the chloride ion layer); (vi) the major positive potential center of lysozyme, especially the Arg128 residue, plays a vital role in leading the adsorption of lysozyme on charged surfaces; (vii) when the solution ionic strength is high, a counterion layer is formed above the positively charged surface, which is the key factor why lysozyme can adsorb on a like-charged surface. Besides, it can provide a plane for many other charged residues anchoring, and there is no need to penetrate the water layer, which declines the protein adsorption stability.

In general, CGMD simulation based on the BMW-MARTINI force field can be used to accurately explore protein adsorption phenomena on most kinds of solid surfaces, especially on charged surfaces. Furthermore, the greatest advantage of BMW-MARTINI is its computational efficiency. It is about 100 times faster than atomistic simulations. In a word, a more efficient method has been displayed here, which enables us to understand the interfacial adsorption mechanism of biomacromolecules on the mesoscopic microsecond time scale.

AUTHOR INFORMATION

Corresponding Author

*E-mail: jianzhou@scut.edu.cn.

Notes

The authors declare no competing financial interest.

ACKNOWLEDGMENTS

Support from the National Key Basic Research Program of China (No. 2013CB733500), the Program for New Century Excellent Talents in University (NCET-07-0313), National Natural Science Foundation of China (Nos. 21376089, 91334202), Guangdong Science Foundation (No. S2011010002078), and the Fundamental Research Funds for the Central Universities (SCUT-2013ZM0073) is gratefully acknowledged. Allocation time from the SCUTGrid at South China University of Technology is gratefully acknowledged.

REFERENCES

(1) Rabe, M.; Verdes, D.; Seeger, S. *Adv. Colloid Interface Sci.* **2011**, *162*, 87−106.
(2) Sheng, Y.-J.; Tsao, H.-K.; Zhou, J.; Jiang, S. Y. *Phys. Rev. E* **2002**, *66*, 011911.
(3) Zhou, J.; Chen, S. F.; Jiang, S. Y. *Langmuir* **2003**, *19*, 3472−3478.
(4) Xie, Y.; Zhou, J.; Jiang, S. Y. *J. Chem. Phys.* **2010**, *132*, No. 065101.
(5) Liu, J.; Liao, C. Y.; Zhou, J. *Langmuir* **2013**, *29*, 11366−11374.
(6) Holmlin, R. E.; Chen, X. X.; Chapman, R. G.; Takayama, S.; Whitesides, G. M. *Langmuir* **2001**, *17*, 2841−2850.
(7) Ostuni, E.; Chapman, R. G.; Holmlin, R. E.; Takayama, S.; Whitesides, G. M. *Langmuir* **2001**, *17*, 5605−5620.
(8) Liu, H. Y.; Zhou, J. *Prog. Chem.* **2012**, *24*, 2187−2197.
(9) Fenoglio, I.; Fubini, B.; Ghibaudi, E. M.; Turci, F. *Adv. Drug Delivery Rev* **2011**, *63*, 1186−1209.
(10) Talbert, J. N.; Goddard, J. M. *Colloids Surf., B* **2012**, *93*, 8−19.
(11) Wang, K.; Zhou, C.; Hong, Y.; Zhang, X. *Interface Focus* **2012**, *2*, 259−277.
(12) Dismer, F.; Hubbuch, J. *J. Chromatogr. A* **2007**, *1149*, 312−320.
(13) Dismer, F.; Petzold, M.; Hubbuch, J. *J. Chromatogr. A* **2008**, *1194*, 11−21.
(14) Zhang, A. J.; Xie, Y.; Zhou, J. *Prog. Chem.* **2009**, *21*, 1408−1417.
(15) Satulovsky, J.; Carignano, M. A.; Szleifer, I. *Proc. Natl. Acad. Sci. U.S.A.* **2000**, *97*, 9037−9041.
(16) Fang, F.; Szleifer, I. *Proc. Natl. Acad. Sci. U.S.A.* **2006**, *103*, 5769−5774.

(17) Zhou, J.; Tsao, H. K.; Sheng, Y. J.; Jiang, S. Y. *J. Chem. Phys.* **2004**, *121*, 1050−1057.
(18) Yang, C.; Peng, C. W.; Zhao, D. H.; Liao, C. Y.; Zhou, J.; Lu, X. H. *Fluid Phase Equilib.* **2014**, *362*, 349−354.
(19) Rabe, M.; Verdes, D.; Seeger, S. *J. Phys. Chem. B* **2010**, *114*, 5862−5869.
(20) Raffaini, G.; Ganazzoli, F. *J. Appl. Biomater. Biomech.* **2010**, *8*, 135−145.
(21) Vellore, N. A.; Yancey, J. A.; Collier, G.; Latour, R. A.; Stuart, S. J. *Langmuir* **2010**, *26*, 7396−7404.
(22) Szott, L. M.; Horbett, T. A. *Curr. Opin. Chem. Biol.* **2011**, *15*, 683−689.
(23) Shaw, D. E.; Maragakis, P.; Lindorff-Larsen, K.; Piana, S.; Dror, R. O.; Eastwood, M. P.; Bank, J. A.; Jumper, J. M.; Salmon, J. K.; Shan, Y.; Wriggers, W. *Science* **2010**, *330*, 341−346.
(24) Latour, R. A. *Biointerphases* **2008**, *3*, FC2−FC12.
(25) Zheng, J.; Li, L. Y.; Chen, S. F.; Jiang, S. Y. *Langmuir* **2004**, *20*, 8931−8938.
(26) Zhou, J.; Zheng, J.; Jiang, S. Y. *J. Phys. Chem. B* **2004**, *108*, 17418−17424.
(27) He, Y.; Hower, J.; Chen, S. F.; Bernards, M. T.; Chang, Y.; Jiang, S. Y. *Langmuir* **2008**, *24*, 10358−10364.
(28) Hower, J. C.; He, Y.; Bernards, M. T.; Jiang, S. Y. *J. Chem. Phys.* **2006**, *125*, No. 214704.
(29) Kubiak, K.; Mulheran, P. A. *J. Phys. Chem. B* **2009**, *113*, 12189−12200.
(30) Kubiak, K.; Mulheran, P. A. *Langmuir* **2010**, *26*, 7690−7694.
(31) Kubiak, K.; Mulheran, P. A. *Langmuir* **2010**, *26*, 15954−15965.
(32) Wei, T.; Carignano, M. A.; Szleifer, I. *Langmuir* **2011**, *27*, 12074−12081.
(33) Wei, T.; Carignano, M. A.; Szleifer, I. *J. Phys. Chem. B* **2012**, *116*, 10189−10194.
(34) Marrink, S. J.; Risselada, H. J.; Yefimov, S.; Tieleman, D. P.; de Vries, A. H. *J. Phys. Chem. B* **2007**, *111*, 7812−7824.
(35) Monticelli, L.; Kandasamy, S. K.; Periole, X.; Larson, R. G.; Tieleman, D. P.; Marrink, S.-J. *J. Chem. Theory Comput.* **2008**, *4*, 819−834.
(36) Wu, Z.; Cui, Q. A.; Yethiraj, A. *J. Phys. Chem. B* **2010**, *114*, 10524−10529.
(37) Wu, Z.; Cui, Q.; Yethiraj, A. *J. Chem. Theory Comput.* **2011**, *7*, 3793−3802.
(38) Zhou, J.; Thorpe, I. F.; Izvekov, S.; Voth, G. A. *Biophys. J.* **2007**, *92*, 4289−4303.
(39) Thorpe, I. F.; Zhou, J.; Voth, G. A. *J. Phys. Chem. B* **2008**, *112*, 13079−13090.
(40) Marrink, S. J.; de Vries, A. H.; Mark, A. E. *J. Phys. Chem. B* **2003**, *108*, 750−760.
(41) López, C. A.; Rzepiela, A. J.; de Vries, A. H.; Dijkhuizen, L.; Hünenberger, P. H.; Marrink, S. J. *J. Chem. Theory Comput.* **2009**, *5*, 3195−3210.
(42) Yesylevskyy, S. O.; Schafer, L. V.; Sengupta, D.; Marrink, S. J. *PLoS Comput. Biol.* **2010**, *6*, No. e1000810.
(43) de Jong, D. H.; Singh, G.; Bennett, W. F. D.; Arnarez, C.; Wassenaar, T. A.; Schäfer, L. V.; Periole, X.; Tieleman, D. P.; Marrink, S. J. *J. Chem. Theory Comput.* **2012**, *9*, 687−697.
(44) Lopez, C. A.; Rzepiela, A. J.; de Vries, A. H.; Dijkhuizen, L.; Hunenberger, P. H.; Marrink, S. J. *J. Chem. Theory Comput.* **2009**, *5*, 3195−3210.
(45) Lopez, C. A.; Sovova, Z.; van Eerden, F. J.; De Vries, A. H.; Marrink, S. J. *J. Chem. Theory Comput.* **2013**, *9*, 1694−1708.
(46) Zhong, T.; Ai, P.; Zhou, J. *Fluid Phase Equilib.* **2011**, *302*, 43−47.
(47) Sun, D.; Zhou, J. *AIChE J.* **2013**, *59*, 2630−2639.
(48) Dong, J.; Zhou, J. *Macromol. Theory Simul.* **2013**, *22*, 174−186.
(49) Marrink, S. J.; Tieleman, D. P. *Chem. Soc. Rev.* **2013**, *42*, 6801−6822.
(50) Kubiak, K.; Mulheran, P. A. *J. Phys. Chem. B* **2011**, *115*, 8891−8900.
(51) Ravichandran, S.; Talbot, J. *Biophys. J.* **2000**, *78*, 110−120.
(52) Ravichandran, S.; Madura, J. D.; Talbot, J. *J. Phys. Chem. B* **2001**, *105*, 3610−3613.
(53) Carlsson, F.; Hyltner, E.; Arnebrant, T.; Malmsten, M.; Linse, P. *J. Phys. Chem. B* **2004**, *108*, 9871−9881.
(54) Raffaini, G.; Ganazzoli, F. *Langmuir* **2010**, *26*, 5679−5689.
(55) Anand, G.; Jamadagni, S. N.; Garde, S.; Belfort, G. *Langmuir* **2010**, *26*, 9695−9702.
(56) Xie, Y.; Liao, C.; Zhou, J. *Biophys. Chem.* **2013**, *179*, 26−34.
(57) Zhang, L.; Bai, S.; Sun, Y. *J. Mol. Graphics Modell.* **2011**, *29*, 906−914.
(58) Periole, X.; Marrink, S.-J. The Martini Coarse-Grained Force Field. In *Biomolecular Simulations*; Monticelli, L., Salonen, E., Eds.; Humana Press: New York, 2013; Vol. *924*, pp 533−565.
(59) Fumi, F. G.; Tosi, M. P. *J. Phys. Chem. Solids* **1964**, *25*, 31−43.
(60) Tosi, M. P.; Fumi, F. G. *J. Phys. Chem. Solids* **1964**, *25*, 45−52.
(61) Essmann, U.; Perera, L.; Berkowitz, M. L.; Darden, T.; Hsing, L.; Pedersen, L. G. *J. Chem. Phys.* **1995**, *103*, 8577−8593.
(62) Darden, T.; Pearlman, D.; Pedersen, L. G. *J. Chem. Phys.* **1998**, *109*, 10921−10935.
(63) van der Spoel, D.; Hess, B.; van Buuren, A.; Apol, E.; Meulenhoff, P.; Tieleman, P.; Sijbers, A.; Feenstra, A.; van Drunen, R.; Berendsen, H. J. C. *Gromacs User Manual*, version 4.5; 2010.
(64) Berendsen, H. J. C.; Postma, J. P. M.; van Gunsteren, W. F.; DiNola, A.; Haak, J. R. *J. Chem. Phys.* **1984**, *81*, 3684−3690.
(65) Humphrey, W.; Dalke, A.; Schulten, K. *J. Mol. Graphics* **1996**, *14*, 33−38.
(66) Pettersen, E. F.; Goddard, T. D.; Huang, C. C.; Couch, G. S.; Greenblatt, D. M.; Meng, E. C.; Ferrin, T. E. *J. Comput. Chem.* **2004**, *25*, 1605−1612.
(67) Fears, K. P.; Sivaraman, B.; Powell, G. L.; Wu, Y.; Latour, R. A. *Langmuir* **2009**, *25*, 9319−9327.
(68) Xie, Y.; Liu, M.; Zhou, J. *Appl. Surf. Sci.* **2012**, *258*, 8153−8159.
(69) Cheng, G.; Zhang, Z.; Chen, S.; Bryers, J. D.; Jiang, S. *Biomaterials* **2007**, *28*, 4192−4199.
(70) Roach, P.; Farrar, D.; Perry, C. C. *J. Am. Chem. Soc.* **2005**, *127*, 8168−8173.
(71) Zhou, J.; Lu, X.; Wang, Y.; Shi, J. *Fluid Phase Equilib.* **2002**, *194−197*, 257−270.
(72) Chen, X.; Yang, T.; Kataoka, S.; Cremer, P. S. *J. Am. Chem. Soc.* **2007**, *129*, 12272−12279.
(73) Feng, H.; Zhou, J.; Lu, X. *Acta Chim. Sin.* **2009**, *67*, 2407−2412.
(74) Feng, H.; Zhou, J.; Lu, X.; Fichthorn, K. A. *J. Chem. Phys.* **2010**, *133*, No. 061103.
(75) Derjaguin, B. V. *Acta Physicochim. URSS* **1941**, *14*, 633−662.
(76) Verwey, E. J. W.; Overbeek, J. T. G. *Theory of the Stability of Lyophobic Colloids*; Dover Publications: Mineola, New York, 1999.
(77) Hung, A.; Mager, M.; Hembury, M.; Stellacci, F.; Stevens, M. M.; Yarovsky, I. *Chem. Sci.* **2013**, *4*, 928−937.
(78) Zhao, J.; Wang, Q.; Liang, G.; Zheng, J. *Langmuir* **2011**, *27*, 14876−14887.